The Thermodynamics of Cell Sorting

AUTHOR(S):

Glazier, James A.

CITATION:

Glazier, James A.. The Thermodynamics of Cell Sorting. 物性研究 1996, 65(5): 691-700

ISSUE DATE:

1996-02-20

URL:

http://hdl.handle.net/2433/95675

The Thermodynamics of Cell Sorting

James A. Glazier
Department of Physics
University of Notre Dame
Notre Dame, IN 46556
USA

ABSTRACT: The simple extended Potts model, which approximates the interactions between cells in contact as a uniform, type dependent surface energy and uses a simple Monte Carlo dynamics, is able to reproduce many observed qualitative behaviors of cell aggregates. The motion of single cells in an aggregate is identical to Brownian motion of ideal particles--hence the temperature in the model corresponds to the fluctuation temperature of the cell membrane. Using appropriate experimental parameters allows the model to quantitatively reproduce both normal and partial cell sorting.

1. INTRODUCTION: Our ability to simulate complex biological structures has improved enormously with the introduction of quasi-molecular dynamics calculations like the extended Potts model which handle automatically the mechanics of cell-cell contact interactions. Because these models are lattice based, additional effects like gravity, mitosis (Mombach *et al.*, 1993) or chemotaxis are easy to include. The most impressive example to date being a model of the life cycle of *Dictyostelium discoideum*, which begins with single free floating amoebae, which aggregate, form a mound, segregate into pre-stalk and pre-spore regions, and finally form a wandering slug that explores its own gradient field of cAMP (Saville and Hogeweg, 1995). Plans to use the extended Potts model with multiple cell types to simulate the lymph nodes of the immune system are well advanced (de Boer, 1995).

However, as physicists, we need to investigate the less flashy aspects of cell sorting. In too many cases, physicists have assumed that they can ignore the fundamental processes that underlie biological activity. The result is often simulations which resemble qualitatively their biological target, but which completely miss the fundamental mechanisms, and are thus at best quantitatively useless, and at worst misleading. At the simplest level, we know that the extended Potts model reproduces almost all the qualitative behaviors of cell sorting. However, we need to establish detailed quantitative agreement as well.

We also have to worry whether we are barking up the right tree at all. The extended Potts model is a classic Monte-Carlo simulation obeying Maxwell-Boltzmann statistics. On the other hand, the forces driving cells, derive from a variety of non-equilibrium cytoskeletal mechanisms, most prominently the migration of myosin on and the polymerization and depolymerization of actin filaments. In particular, the simulation has a fluctuation temperature, T, that characterizes the amplitude of surface fluctuations. Cells membranes need not obey such quasithermal distributions. Since the rate of improvement of a pattern exploring a rough energy surface can depend sensitively on the fluctuation spectrum, we need to measure the fluctuations of real cells.

2. CELL SORTING: An early embryo, or even an adult animal such as *hydra,* can regenerate from an aggregate of randomly mixed cells (Holtfreter, 1944, 1947; Townes and Holtfreter, 1947; Armstrong, 1989; Wilson, 1907; Dan-Sohkawa *et al.*, 1986; Noda, 1971; Gierer *et al.*, 1972). Even *in vivo*, during embryonic development or wound healing, cells must migrate long distances (Keller, 1987; Fristrom, 1988; Keller and Hardin, 1987). Biologists tend to think of this migration in terms of its function and the evolutionary pathways which led to it. To a physicist, the intriguing question is the mechanisms which can cause cell migration. A cell can receive

information from its environment through bulk gradients in diffusible substances, through surface properties of neighboring cells or substrates sensed by direct contact, or through external fields such as light or gravity.

Reaction-diffusion, with analogies in chemical systems, flame fronts, and the Belousov-Zhabotinsky reaction (Gierer and Meinhardt, 1972; Turing, 1952) is one classical example of a diffusion mechanism. It may dominate cell differentiation, for example, determining the sequence or the number of digits in the hand. Another is the migration of individual *Dictyostelium discoideum* amoebae up gradients of cAMP, creating spiral waves and DLA-like fractals.

While cell sorting was first observed qualitatively in 1744 (Lenhoff, 1986), its kinetics have only recently been studied quantitatively (Townes and Holtfreter, 1955; Armstrong, 1989; Newman and Comper, 1990; Mombach *et al.*, 1995). Steinberg proposed that cell sorting resulted from energy minimization, the Differential Adhesion Hypothesis (DAH) (Steinberg, 1963). In his theory, adhesion energies are associated with type dependent, *homotypic* (like cell) or *heterotypic* (unlike cell) interfaces and cell-medium interfaces and the minimization of the overall interface energy drives the evolution of the aggregate. Cells rearrange to decrease the total cell-cell contact energy. Thus cell sorting is analogous to the demixing of immiscible liquids. For example, when water is dispersed in oil, surface tension causes the water droplets to merge and form a single droplet. Aggregates of cells obtained from the liver and heart of chick embryos mimic liquid behavior (Foty *et al.*, 1994). However, the DAH says nothing about the dynamics or mechanisms of the minimization.

Non-specific and/or type-dependent surface adhesivity is present in cells from all multicellular organisms in the form of numerous proteins outside or across the membrane. Common adhesive molecules like N-CAM are related (possibly evolutionary precursors) to immunoglobins, and share their repeated highly variable recognition sequences (Takeichi, 1991). Thus a cell which expresses several N-CAM like molecules can vary its adhesivity with respect to other cell types almost independently. This mechanism allows genetics, as expressed in the choice of recognition sequences during cell differentiation to directly influence organization, perhaps, via homeotic gene pathways.

Gradually, the physics of cell rearrangement is becoming clear. The energy surface explored by the cells has weak local minima (Mombach *et al.*, 1995). Random cell-membrane fluctuations allow each cell to locally explore its neighborhood and diffuse to the minimum energy configuration (Armstrong, 1989; Phillips and Davis, 1978).

3. CELL SORTING EXPERIMENTS: The typical experiment selects two cell types, e.g. the pigmented and neural retinal cells of chicken embryo or the endodermal and ectodermal cells of *hydra*. If necessary, one cell type is stained. The tissues are then dissociated into single cells, mechanically and/or chemically, mixed in the desired proportion, reaggregated into a random cluster, and cultured either in hanging drops, shaker flasks (chicken) or culture wells (*hydra*). The dissociation destroys any preexisting diffusible gradients. Thus, initial cell migration depends only on cell-cell surface recognition. If the dissociation procedures preserves surface adhesion molecules, cell migration begins immediately. Otherwise they must reform, and migration begins after a few hours.

4. SIMULATIONS: We use an extended Potts model on a 100^3 or 200^3 third neighbor square lattice (Graner and Glazier, 1992), with a spin, $\sigma(i,j)$, defined at each lattice site, (i,j). We assign a separate spin, σ, to each of the cells in the pattern, with all lattice sites with a given σ composing the cell σ. Each cell typically contains a few hundred lattice sites.

Each cell has an associated cell type $\tau(\sigma)$. Bonds between like spins have energy 0, so the energy inside a cell is zero. Mismatched spins at cell boundaries contribute a cell type dependent surface energy $J(\tau,\tau')$. We include the cell size as a type dependent target volume, A_τ, with membrane elasticity, λ. The total energy is thus:

$$\mathcal{H}_{\text{Sort}} = \sum_{(i,j)(i',j')\ \text{Neighbors}} J\left(\tau(\sigma(i,j)),\tau(\sigma(i',j'))\right)\left(1-\delta_{\sigma(i,j),\sigma(i',j')}\right)+ \lambda \sum_{\text{Spins}\ \sigma}\left(a(\sigma)-A_{\tau(\sigma)}\right)^2, \quad (1)$$

where $a(\sigma)$ is the volume of a cell σ. The cell types are low surface energy, **dark**, cells, high surface energy, **light**, cells and a fluid medium of unconstrained volume.

The initial condition is a random round aggregate: to obtain it, we begin with an array of rectangular cells of a single cell type and allow it to round; we then randomly reassign the cell types. We evolve using a standard Monte Carlo Boltzmann algorithm at fixed temperature, allowing the nucleation of medium filled vacancies but not heterogeneous cells. The probabilty of a change:

$$P\left(\sigma(i,j)\rightarrow\sigma'(i,j)\right)=\begin{cases}1: \Delta\mathcal{H}<0\\ e^{\frac{-\Delta\mathcal{H}}{T}}: \Delta\mathcal{H}>0\end{cases}, \quad (2)$$

where, T, is the fluctuation temperature and $\Delta\mathcal{H}$is the energy change caused by the spin flip. One Monte Carlo step (MCS) is 16 times as many time steps as there are lattice sites.T in the simulation corresponds not to the thermal membrane fluctuations, which are too small to be relevant (Graner, 1993), but to the much bigger cytoskeletally driven membrane fluctuation amplitude. We can distinguish three temperature regimes: low-temperature freezing, a "normal" regime which is qualitatively independent of the temperature, and a high temperature disordered regime. The existence of this broad normal band suggests that the lattice anisotropy is not too important and that we are seeing the true local minima of the pattern.

The model is simple but realistic, in that the position and diffusion of the membrane determine the dynamics as they do for real loosely aggregated cells. Relative contact energies and boundary curvatures drive all motion. Thus vertices are always close to their equilibrium condition and all topological rearrangements happen automatically and rapidly.However, the cells are nonpolar, whereas real cells in two-dimensional tissues (epithelia) have strongly orientation dependent mechanical and adhesive properties. More seriously, the cell-cell adhesivity is time independent. In actual cell-cell contact, adhesion usually increases with time.

5. SINGLE CELL DIFFUSION: Cell locomotion occurs through cytoskeletally driven contractions and expansions of the cell membrane. Adding Cytochalasin B to the culture medium or holding the cells at 4°C reversibly blocks cytoskeletal activity, stopping locomotion, but not permanently damaging the cells. We found that the presence of Cytochalasin B in the culture medium yields results equivalent to those obtained from the simulation at low T, Suggesting that membrane fluctuations in aggregates of biological cells play a role analogous to temperature in ordinary thermodynamics.

However, the fluctuation spectrum for real cells need not be same as the Monte Carlo/Boltzmann fluctuations in the model. Different fluctuation spectra might lead to substantially different rates of sorting and non-thermodynamic behaviors in the biological aggregate. We therefore must establish the validity of our thermodynamic model.

To eliminate possible bias to the cell motion due to long range diffusible chemotactic agents which could be released by either cell type, we used a random mixture of neural retinal cells with either a single or a few very widely spaced pigmented retinal cells per aggregate, in a ratio of about 10^4 neural retinal cells to each pigmented retinal cell. Since the spectra for random walks in two and three dimensions are the same, (Hug *et al.*, 1995; Doolittle *et al.*, 1995) we recorded the two dimensional projection of the three dimensional motion of a set of five pigmented retinal cells in the aggregate for 30 hours corrected to eliminate bulk motion of the sample. The widely separated pigmented cells do not migrate towards each other, ruling out chemotaxis due to pigmented cell signaling.

The averaged power spectrum of position versus time for each coordinate for all cells is linear with slope 1.8±0.1 over 1 1/2 decades close to that for an extended Potts model simulation of a single dark cell in a light aggregate (slope 1.6±0.07) and a simulation of a discrete pseudo-random walk with 2^{14} steps (slope 1.82±0.01), while an infinite random walk has slope 2.0. Because the projection of a random walk is also a random walk, the result confirms our decision to neglect the third dimension.

The temporal autocorrelation of the velocity for both experiment and theory has a single narrow peak at a lag of 0, approximating a delta function. The correlation time for the velocity was shorter than the measurement interval for both experiment (30 minutes) and simulation (5 MCS), agreeing with the hypothesis of time-uncorrelated velocities in Brownian motion.

The effective diffusion constant, D, is given by the relation:

$$\langle z^2 \rangle = 2Dt, \qquad (3)$$

where t is the time, and z is the average between x and y displacements for the cells. Typically D=1.9±0.1μm^2/hour, much smaller than the diffusion constant of gases in normal liquids, which is typically 360μm^2/hour.

In figure 3 we present a histogram for the velocity distribution of the cells, obtained by summing the histograms of individual cells. We fit them to the Maxwell distribution for the velocity of random particles in a gas in two dimensions (Reif, 1965):

$$F(v) = a_0 v \exp(a_1 v^2). \qquad (4)$$

Both simulated and experimental distributions agree within counting error to the Maxwell distribution, though poor statistics results in larger errors for the experimental data.

Thus, in the absence of external biases, the cells behave in both simulation and experiment as ideal thermodynamic particles, executing a random walk with temporally uncorrelated velocity and a Maxwellian velocity distribution, justifying our use of a quasi-thermal formulation in our simulations. Aggregates round in the same way that a liquid drop rounds; cells perform a biased random walk guided by energy minimization in a manner identical to simple liquids. Spherical symmetry results from simple energy minimization.

6. CELL SORTING: Cell sorting is the classic behavior of mixed heterotypic aggregates. In figure 2 we show the sorting of neural (light) and pigmented (dark) retinal cells from seven day chicken embryos (Armstrong, 1989; Steinberg, 1970). The initially free floating cells (a) gradually coalesce to form a random aggregate (b). During the next few hours a surface light monolayer begins to form (c) and the aggregate rounds. Even after the monolayer is complete, the dark cell clusters in the bulk remain small (d). These clusters gradually coalesce (e) until only a single dark cell cluster surrounded by light cells remains (f). The central cluster is often not centered in the aggregate (Steinberg 1963). Similar sorting occurs in *hydra* (Noda, 1971; Gierer *et al.*, 1972), and in two-dimensional monolayers (Garrod and Steinberg, 1975; Steinberg and Garrod, 1975; Nicol and Garrod, 1979, 1982).

In figure 1 we show a simulation beginning with a random aggregate (a'). Isolated cells are rapidly expelled and small clusters form within ten MCS (b') and white cells rapidly begin to fill the boundary (b). By 70 MCS the surface monolayer is almost complete (c) and the black cells form a connected cluster (c'). From this point on, the sorting slows greatly. At 300 MCS only one unconnected white cell cluster remains (d') and this reconnects by 400 MCS (e'). The final rounding of the dark cell cluster is very slow (f'), and is not completed by 2500 MCS.

7. QUANTITATIVE EXPERIMENTS: To verify that the simulation agrees quantitatively with the experiment we must first estimate the experimental values of the simulation parameters, including temperature and surface energy.

The surface tensions in the simulation are (Glazier and Graner, 1993): $\sigma(l,l)=4.5$ for light-medium interface, $\sigma(d,d)=7.0$ for dark-medium interface, and $\sigma(d,l)=0.5$ for dark-light interface which yields a ratio between light-medium and dark-medium surface tensions of 0.64. The experimental surface tensions for liver and heart cell aggregates of chick embryos are 4.3± 0.1dyn/cm and 8.3± 0.1dyn/cm, respectively which yields a ratio of 0.52 (Foty *et al.*, 1994). For ectodermal and endodermal cells of *Hydra vulgaris* this ratio is estimated to be 0.6 (Sato-Maeda *et al.*, 1994). Unfortunately, in these experiments the surface tensions in the heterotypic cell interface were not measured.

Since fractional boundary lengths depend on the ratios and relative size of the different types of cells, we set the parameters in the simulation to the corresponding experimental values. The average diameter of almost spherical cells is approximately 5μm (±0.3μm) for neural retinal cells and 9μm (± 1.6μm) for pigmented retinal cells, which yields a volume ratio of approximately 5.8. In the simulation, the typical volume of light cells is 100 sites, of dark cells 580 sites. Completely sorted aggregates have approximately 30 neural retinal cells for each pigmented retinal cell, a ratio we employ in the simulation.

To simulate normal sorting we set, $T=32$, giving typical fluctuations of ~ 1 lattice site corresponding to experimentally observed fluctuations of about 1μm (Graner, 1994) for cells with a diameter of 5-10μm. At $T=0$ the simulated aggregates do not evolve in time due to residual lattice anisotropy (Glazier and Graner, 1993). Since cell membranes fluctuate due to real temperature at an amplitude of roughly a tenth of the normal cytoskeletally driven fluctuations (Graner, 1995) in the presence of Cytochalasin B, we set $T=4$.

We monitored aggregation by taking images at regular time intervals of normal sorting and sorting in the presence of 10μg/ml Cytochalasin B. Aggregates of the same size form in the same time in the presence or absence of Cytochalasin B. The images obtained from the experimental aggregates are two-dimensional vertical projections of a three-dimensional structure. In the simulation we project the aggregate onto a plane, by scanning the columns of the three-dimensional matrix. A column with a dark cell generates a dark site on the projected plane, a column composed only of light cells generates a light site, and only of medium generates a medium site. With this algorithm all dark cells in our simulated aggregates are visible, while some experimental cells are not, introducing a small error (<10%) in our measured boundary length. This difference decreases in time to zero for aggregates that sort completely.

The aggregates we studied ranged in diameter from 150 to 300μm and the estimated number of cells from $2 \bullet 10^4$ to $8 \bullet 10^4$. Cytochalasin B resulted in partial sorting. The aggregates were not rounded, a complete light layer and an internal dark core did not form, though some dark cells clustered. The simulation at $T=4$ resembles the experiment.

At T=32 sorting is complete,. In figure 4(a) and (b) we plot the time evolution of the boundaries between 5 and 87 hours for partial and normal sorting, respectively. Points represent the average of 2-6 different aggregates. The time in the simulation was rescaled to real time in the experiment by the best coincidence between order parameters at early and late stages. In partial sorting the dark-medium boundary quickly decreases in the initial 4 hours and then becomes constant as a partial light cell surface layer forms. The light-medium and dark-light boundaries increase in the initial 4 hours due to the decrease of the dark-medium boundary and then remain constant. In normal sorting the dark-light boundary decreases as both cell types segregate and the light-medium boundary increases while the dark-medium boundary decreases, as a result of the formation of the light cell layer, until they reach plateaus. The formation of the external light cell layer is much faster than the characteristic time of the whole sorting process. In normal sorting, the curves are predominantly logarithmic.

8. CONCLUSION: The agreement between the thermodynamic simulation and cell sorting appears to be more than coincidental. Our simple model of isotropic cells, including only differential surface energies and an area constraint, can reproduce all of the sorting behaviors of random aggregates. Thus, the energy landscape suffices to explain many aspects of biological cell sorting. When we reproduce the experiemntal parameters in the simulation, the two evolve in quantitative agreement.

Single pigmented cells in neural cell aggregates behave, in both experiment and simulation, as ideal gas molecules with time uncorrelated Maxwell distributed velocities. Thus the use of a temperature in the simulation to mimic cell membrane fluctuations is justified, though we must still establish that the effective temperature of the different cell types is the same. Small membrane fluctuations suffice to find the optimal configuration, though the energy surface has weak local minima that trap in the absence of fluctuations. As a consequence, the system can overcome energy barriers and explore ergodically the energy space to reach its global minimum. Engulfment, in which the light and dark cells are brought together as coherent tissues, should have much smaller energy barriers. We would expect that engulfment would proceed normally, though more slowly, regardless of the presence of Cytochalasin B.

We need better measurements of the adhesivity of cells and cell-medium surface tensions in real aggregates. We are currently measuring the fluctuation amplitude and spectrum. Initial results indicate that the cytoskeletal fluctuations are quasithermal in spectrum (Zajac *et al.*, 1995). The simulation is being improved to describe more complex biological behavior like the early stages of an embryo (blastulation) by increasing the number of different types of cells and introducing mitosis (Mombach *et al.*, 1993). The current work suggests a quantitative study of the cell motion *in situ* in the gastrulating phase of embryo formation to verify whether cells move deterministically or randomly during the construction of the ecto, meso and endodermal tissues.

ACKNOWLEDGMENTS: This research has been supported by National Science Foundation grant DMR 92-57011, the Ford Motor Company, the American Chemical Society/Petroleum Research Fund and the Exxon Educational Foundation.

REFERENCES:

Armstrong P. B., *Crit. Rev. Biochem. and Mol. Biol.* **24** (1989) 119.

de Boer R., personal communication (1995).

Dan-Sohkawa M., Yamanaka H., and Watanabe K., *J. Embryol. exp. Morph.* **94** (1986) 47.

Doolittle K. W., Reddy I. and McNally J. G., *Developmental Biology* **167** (1995) 118.

Fristrom D., *Tissue & Cell* **20** (1988) 645.

Foty R. A., Forgacs, G., Pfleger, C. M. and Steinberg M. S. , *Phys. Rev. Lett.* **72** (1994) 2298.
Garrod D. R. and Steinberg M. S., *Nature* **244** (1973) 568.
Gierer A. and Meinhardt H., *Kybernetik* **12** (1972) 30.
Gierer A., Berking S., Bode H., David C. N., Flick K., Hansmann G., Schaller H. and Trenkner E., *Nature New Biol.* **239** (1972) 98.
Glazier J. A. and Graner F., *Phys. Rev. E* **47** (1992) 2128.
Glazier J. A., Raphael R. C., Graner F. and Sawada Y., to appear in Interplay of Genetic and Physical Processes in the Development of Biological Form, eds. D. Beysens, M.-A. Felix, G. Forgacs, F. Gaill (Springer, 1995).
Graner F. and Glazier J. A., *Phys. Rev. Lett.* **69** (1992) 2013.
Graner F. and Sawada Y., *J. theor. Biol.* **164** (1993) 477.
Graner F., *J. theor. Biol.* **164** (1993) 455.
Graner F., (1995), private communication.
Holtfreter J., *J. Morph.* **80** (1947) 25.
Holtfreter J., *Rev. Can. Biol.* **3** (1944) 220.
Hug C., Jay P. Y., Reddy I., McNally J. G., Bridgeman P. C., Elson E. L., and Cooper J. A., *Cell* **81** (1995) 591 .
Keller R. and Hardin J., *J. Cell Sci. Suppl.* **8s** (1987) 369.
Keller R., *Zool. Science* **4** (1987) 763.
Lenhoff S.G., Hydra and the Birth of Experimental Biology - 1744, (The Boxwood Press, Pacific Grove, 1986).
Mombach J. C. M., de Almeida R. M. C., and Iglesias J. R., *Phys. Rev. E* **48** (1993) 598.
Mombach J. C. M., Glazier J. A., Raphael R. C. and Zajac M.,*Phys. Rev. Lett.* **75** (1995) 2244.
Mombach J. C. M. and Glazier J. A., submitted to *Phys. Rev. Lett.* (1995).
Newman S. A. and Comper W. D., *Development* **110** (1990) 1.
Nicol A. and Garrod D. R., *J. Cell Sci.* **38** (1979) 249.
Nicol A. and Garrod D. R., *J. Cell Sci.* **54** (1982) 357.
Noda K., *Zool. Mag.* **80** (1971) 99.
Phillips H. and Davis G., *Am. Zool.* **18** (1978) 81.
Reif F., Fundamentals of Statistical and Thermal Physics, (McGraw-Hill, Inc., New York, 1965).
Sato-Maeda M., Uchida M., Graner F. and Tashiro H., *Devel. Bio.* **162** (1994) 77.
Saville N. and Hogeweg P., unpublished (1995).
Steinberg M. S., *Science* **141** (1963) 401.
Steinberg M. S. and Garrod D. R., *J. Cell Sci.* **18** (1975) 385.
Steinberg M. S., *J. Exp. Zool.* **173** (1970) 395.
Takeichi M., *Science* **251** (1991) 1451.
Townes P. and Holtfreter J., *J. exp. Zool.* **128** (1955) 53.
Turing A. M., *Phil. Trans. Roy. Soc. Lond.* **B237** (1952) 37.
Wilson H., *J. Exp. Zool.* **5** (1907) 245.
Zajac M., Upadhyaya A., Raphael R. and Glazier J. A., preprint (1995).

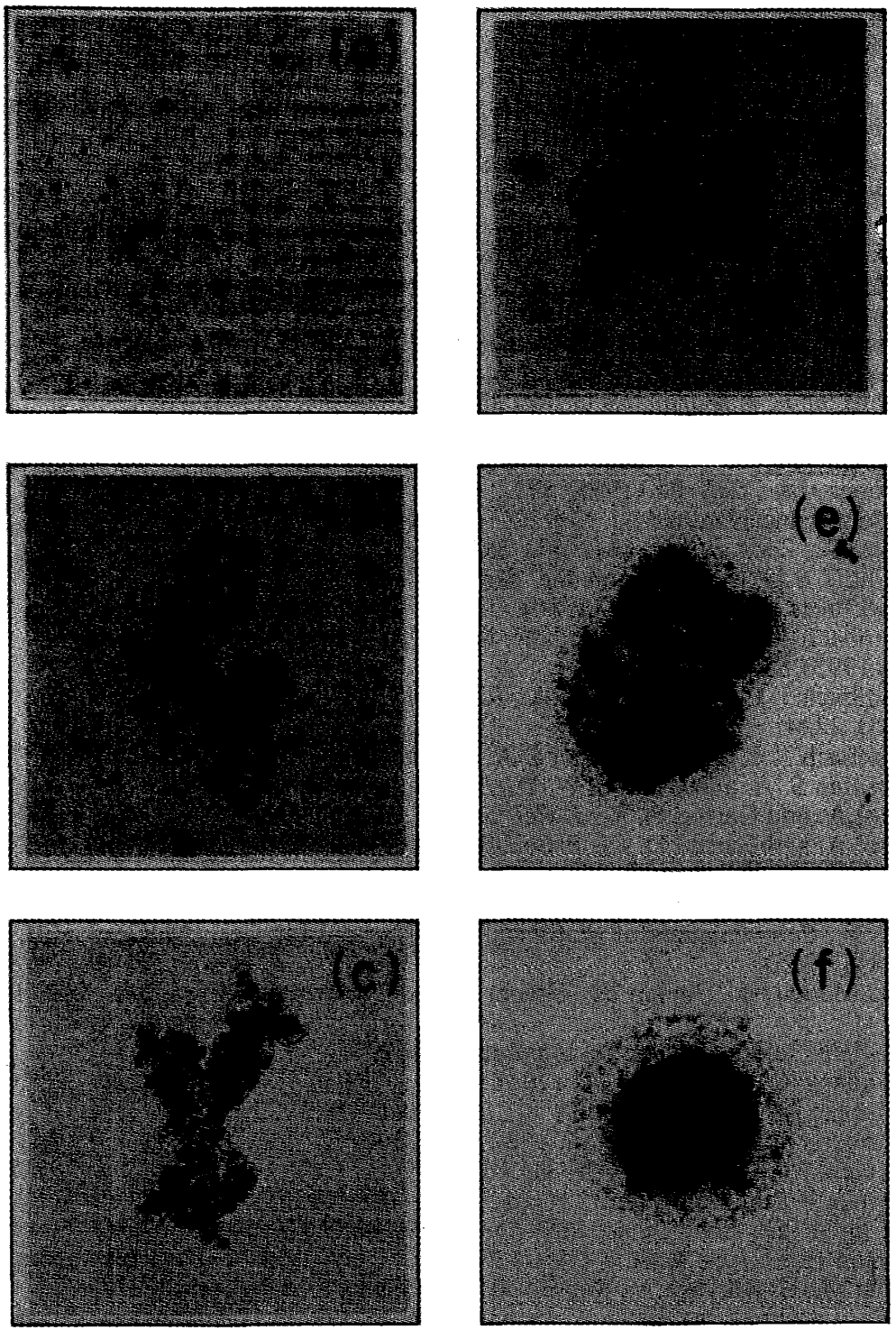

Figure 1. Simulation of Three Dimensional Cell-sorting. (a, a') Initial configuration: random aggregate. (b, b') 10 MCS. (c, c') 70 MCS. (d, d') 300 MCS. (e, e') 400 MCS. (f, f') 2500 MCS. Parameters: J_{ll}=7, J_{dd}=2, J_{ld}=5, J_{lM}=J_{dM}=8, T=32, λ=1. From (Glazier *et al.*, 1995).

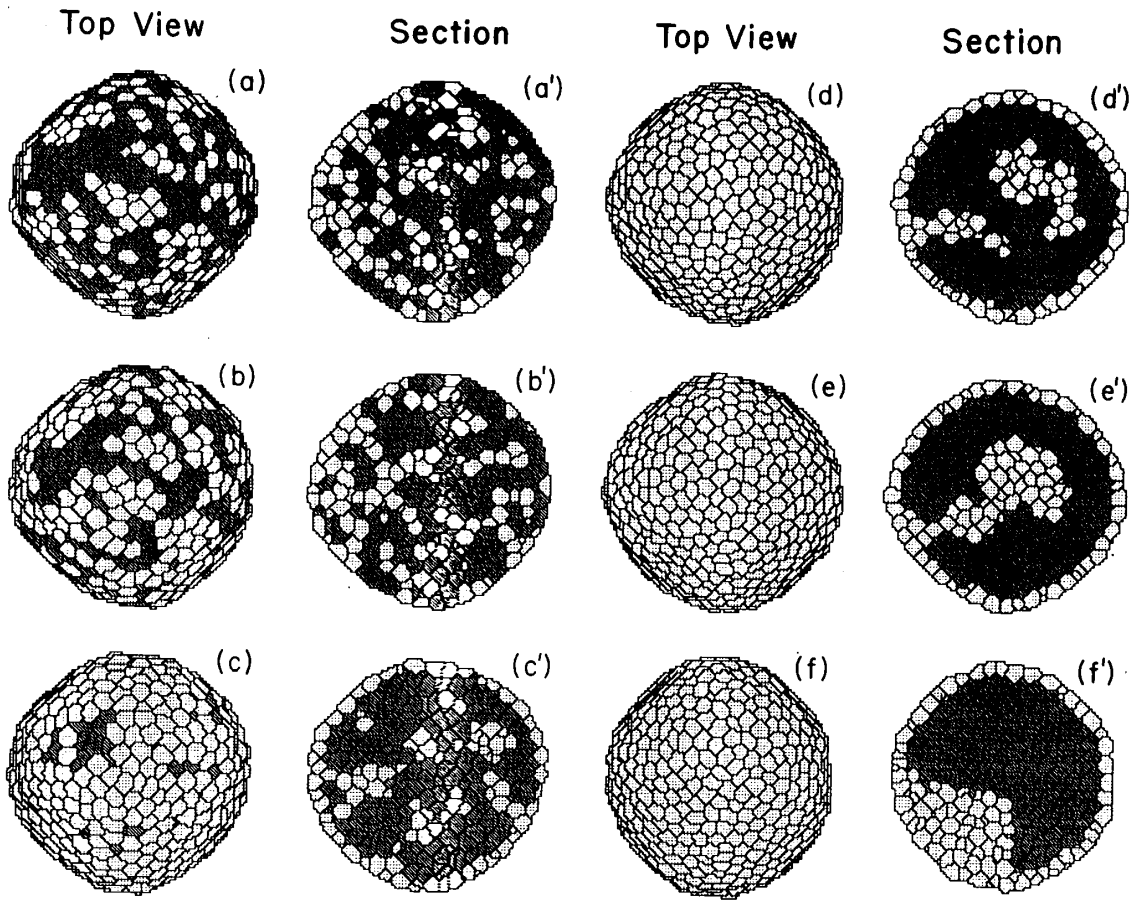

Figure 2. Cell sorting between pigmented (dark) and neural (light) retinal cells in 7th day chick embryo in three dimensional aggregates. (a) Initial dissociated cells. (b) Formation of random aggregate (7 hours). (c) Monolayer formation (8 hours). (d) Rounding of aggregate, completion of surface layer (15 hours). (e) Bulk sorting (60 hours). (f) Final sorted state (>60 hours). Pictures show top views of several different three dimensional aggregates. From (Glazier *et al.*, 1995).

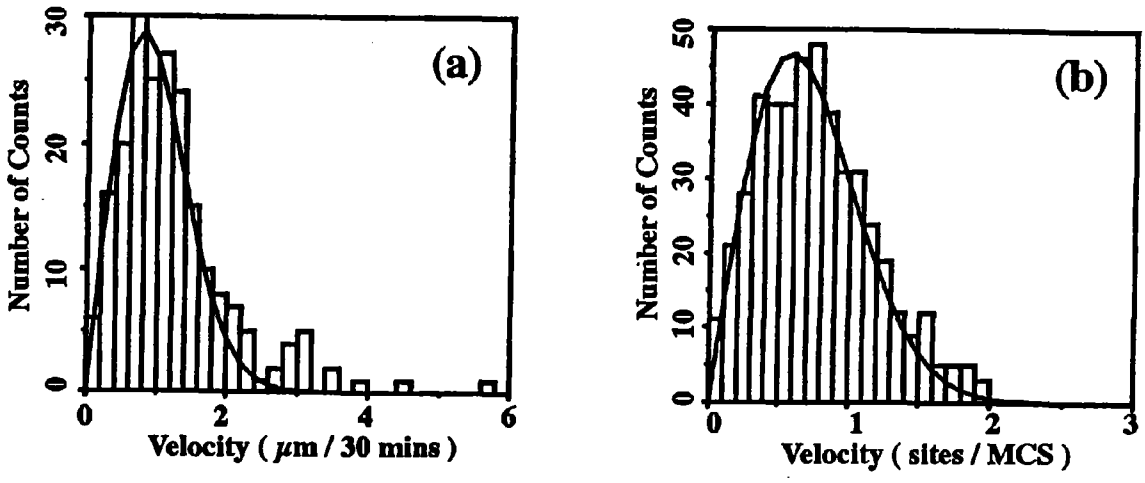

Figure 3. Histogram of the two-dimensional cell velocity distribution for (a) experiment and (b) simulation. The solid curve is a fit of the Maxwell distribution (equation 3). From (Mombach and Glazier, 1995).

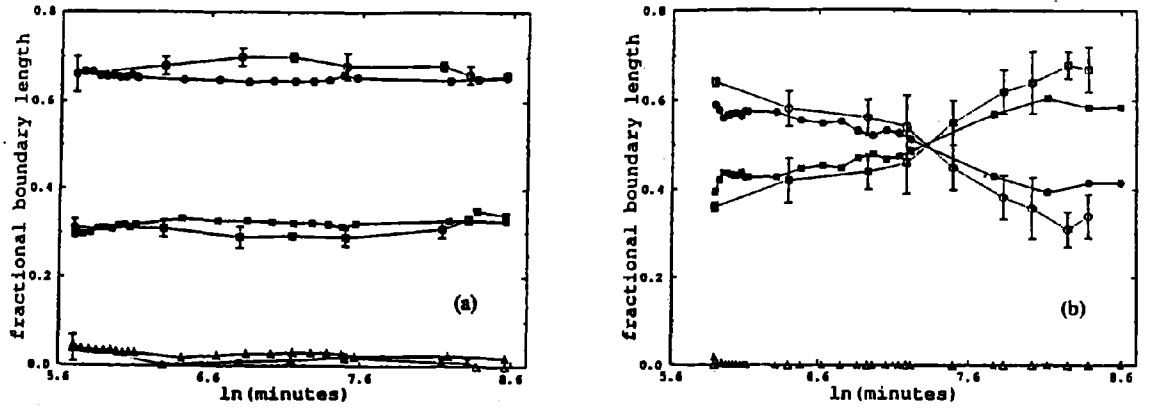

Figure 4. Time evolution of boundaries lengths for partial (a) and complete (b) cell sorting for experiment (open symbols) and simulation (closed symbols). Circles, boundary between dark and light cells. Squares, boundary between light cells and medium. Triangles, boundary between dark cells and medium. Error bars are one standard deviation. From (Mombach *et al.*, 1995).